Salient Frame Detection for Molecular Dynamics Simulations

Robert Patro, Youngmin Kim, Cheuk Yiu Ip,* Andriy Anishkin,
Sergei Sukharev**, Dianne P. O'Leary, and Amitabh Varshney

University of Maryland, College Park MD 21044, USA

Abstract. Saliency-based analysis can be applied to time-varying 3D datasets for the purpose of summarization, abstraction, and motion analysis. As the sizes of time-varying datasets continue to grow, it becomes more and more difficult to comprehend vast amounts of data and information in a short period of time. Automatically generated thumbnail images and previewing of time-varying datasets can help viewers explore and understand the datasets significantly faster as well as provide new insights. In this paper, we introduce a novel method for detecting salient frames for molecular dynamics simulations. Our method effectively detects crucial transitions in simulated mechanosensitive ion channel (MscS), in agreement with experimental data.

1 Introduction

Recent advances in acquisition and simulation techniques have generated a huge amount of time-varying datasets. Time-varying data can be acquired from scientific simulation, videos, and animation libraries. Features in the time-varying datasets are commonly defined as the regions of interest that a human observer is likely to look for. As the number and complexity of these datasets increase exponentially [1], it is becoming impractical to expect a human observer or a domain expert to discover all the features manually. Automatic or semi-automatic tools to help humans discover scientifically interesting features are especially important for this reason.

Many illustration-based techniques have been proposed by several researchers [2–4] to summarize time-varying datasets such as ocean flow, volume, and human skeletons. The basic step for these illustration techniques is automatic detection of salient frames which have interesting features. In the method of image saliency by Itti *et al.* [5] or mesh saliency by Lee *et al.* [6], they use a center-surround operator to identify the uniqueness of a pixel or a vertex with respect to its neighborhood. In this paper, we have decided to use a similar approach and define saliency as the uniqueness of a single frame with respect to its neighboring frames both forwards and backwards in time. Our

* Youngmin Kim, Rob Patro, Cheuk Yiu Ip, Dianne P. O'Leary and Amitabh Varshney are with the University of Maryland Department of Computer Science and University of Maryland Institute for Advanced Computer Studies (UMIACS) E-mail: {rob,ymkim,ipcy,oleary,varshney}@cs.umd.edu.

** Andriy Anishkin and Sergei Sukharev are with the Department of Biology, University of Maryland, College Park, MD 20742. E-mail: anishkin@icqmail.com, sukharev@umd.edu.

collaborator, Dr. Sergei Sukharev's group at Biology Department at the University of Maryland, was interested in identifying the frames in molecular dynamics simulations, where the anomalies (kinks) in the secondary structures happen in the opening and closing simulations of the *E. coli* channel [7]. We validate the effectiveness of our salient frame detection algorithm in this molecular dynamics simulation.

The rest of this paper is organized as follows. A review of related work is provided in Section 2. In Section 3, we formulate the relationship between one residue and the neighboring residues in space, and present an algorithm to detect saliency in time. Results are presented in Section 4. Section 5 concludes this paper and discusses future work.

2 Background and Related Work

The goal of this paper is to detect salient frames in molecular dynamics simulations. This section briefly reviews some background in protein and ion channel structure and the related research in the area of motion analysis and visualization for time-varying 3D datasets.

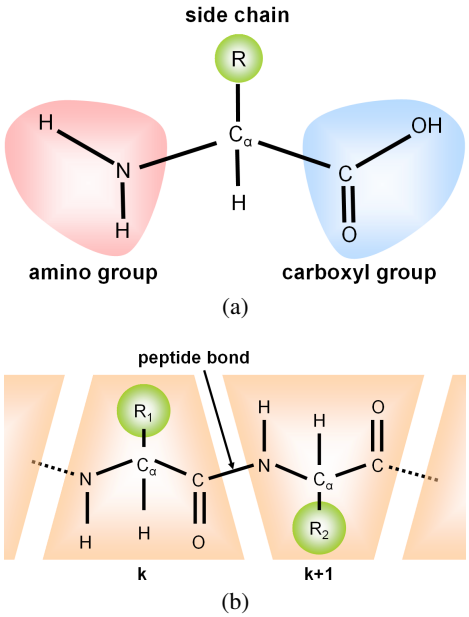

Fig. 1: *Image (a) shows the structure of an amino acid. Image (b) shows a peptide bond formed by the reaction between a carboxyl group of one amino acid and an amino group of the other amino acid. Images are adapted from [8].*

2.1 Protein Structures

A protein structure is formed by a unique three-dimensional assembly of a specific polypeptide chain. Each polypeptide chain contains a particular sequence of serially linked amino acids. Figure 1(a) shows an amino acid which is composed of an amino group, a carboxyl group, and a side-chain, which are connected at the central C_α atom. When the carboxyl group of one amino acid reacts with the amino group of another amino acid, a peptide (i.e., amide) bond (Figure 1(b)) is formed by releasing a molecule of water (H_2O). This peptide bond is typically composed of four atoms (C, O, N, and H) which lie on a common plane due to the partial double bond characteristic at the CO-NH connection. Here, the recurring atomic array of N-C_α-C(=O) from each amino acid of a polypeptide chain constitutes the protein *backbone*. By definition, the specific amino acid sequence for each polypeptide chain is the *primary* structure of the protein. Segments of polypeptides often fold locally into stable structures such as α-helices or β-strands, each of which is called a *secondary* structure. An α-helix is a right-handed coiled conformation, resembling a spring. β-strands connected laterally by three or more hydrogen bonds, form a generally twisted, pleated sheet.

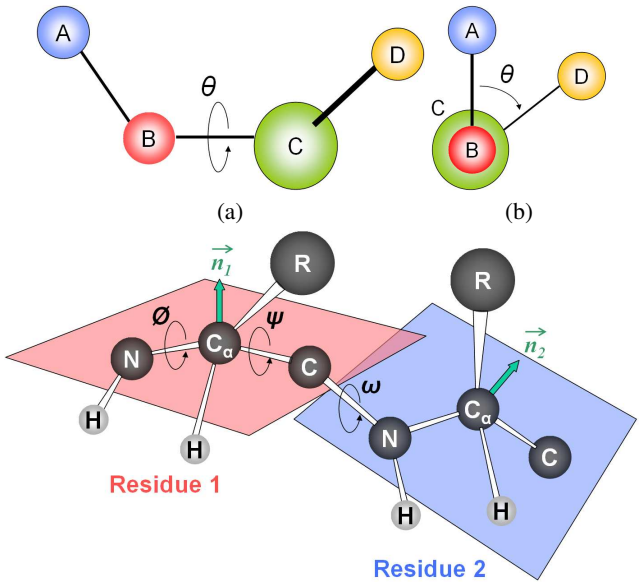

Fig. 2: *Images (a) and (b) show the computation of a dihedral angle between 4 atoms (A, B, C, and D). When we align the atom B and the atom C as shown in Image (b), the dihedral angle θ is defined as the angle between the atom A and the atom D in clockwise direction. Image (c) shows the dihedral angles (ϕ between C-N-C_α-C, ψ between N-C_α-C-N, and ω between C_α-C-N-C_α) and the normal vectors (n_1 and n_2 on the planes defined using N-C_α-C in residue 1 and residue 2, respectively. Images are adapted from [8].*

The angle between two planes is referred as their *dihedral* angle. Figure 2(a) and (b) shows how we can compute the dihedral angle when there are four atoms which are not co-linear in 3D space. We first align the atoms *B* and *C* as shown in Figure 2(b). Then the dihedral angle corresponds to the angle measured in clockwise direction between the atom *A* and the atom *D*. Similarly, for a sequence on a protein's polypeptide chain, backbone atoms (C, N, and C_α) allow for three different dihedral angles of proteins as depicted in Figure 2(c): ϕ involving the backbone atoms C-N-C_α-C, ψ involving the backbone atoms N-C_α-C-N, and ω involving the backbone atoms C_α-C-N-C_α. The planarity of the peptide bond usually restricts ω to be 180° or 0°. Thus the Ramachandran plot [9] considers two variable dihedral (torsion) angles (ϕ and ψ) and shows possible combinations of these conformational angles of representative secondary structures in a polypeptide such as α-helices or β-sheets.

2.2 Ion Channels

Ion channels are proteins that regulate the flow of ions into and out of the cells. Ion channels enable a very rapid flow of ions. In physiological conditions, MscS can provide for the flow of about a billion ions per second. Ion channel transitions are very fast – some opening for less than a millisecond before they close. This rapid and highly specific gating of ion channels is necessary for survival of cells. The ion channel kinetics impacts the speed at which ions flow across the cell membrane and the reaction time of a nerve or a muscle cell, and thus dictates the response time of the animal to the possible environmental dangers. An accurate understanding of the structural changes and functioning of ion channels is vital for therapeutic drug design. Nearly a third of the top 100 pharmaceutical drugs target ion-channels.

The bacterial mechanosensitive channel MscS and its eukaryotic homologs are principal turgor regulators in many walled cells. In bacteria, both free-living and pathogenic, these channels play critical roles of tension-driven osmolyte release valves thus allowing the organisms to avoid osmotic rupture in the event of abrupt medium dilution. MscS opening is driven directly by tension in the surrounding lipid bilayer and is accompanied by tilting of the pore-lining helices (TM3) which assume a kink-free conformation [10]. When tension is released, the TM3 helices may buckle at two different hinge points, which defines the progression toward the closed state, which is shown in figure 3(a). Thus, helical flexibility appears to define the functional cycle of *E. coli* MscS. The major dataset analyzed consisted of two trajectories of atomic coordinates obtained from 4 *ns* steered simulations representing opening of wild-type and F68S mutant of *E. coli* MscS. The major goal was identification of frames in which conformations of helices deviated from the typical alpha-helical conformations.

2.3 Saliency-based Motion Analysis

Designers and artists have long used a single static image or a few images to illustrate dynamics of scenes for motion. They have depicted dynamics to facilitate visual communication in comic books and storyboards [11]. Recently, several graphics researchers [3, 12, 13] have proposed illustration-based techniques to depict the dynamics of time-varying data in a compact way. They use principles of visual art such as

glyphs, and generate an image (or a few images) to summarize the time-varying data to facilitate visual communication. For instance, Joshi and Rheingans [3] have used illustration-based techniques such as speedlines, flow ribbons, and strobe silhouettes to convey change over time for a time-varying dataset. Nienhaus and Dollner [12] have used dynamic glyphs such as directed acyclic graphs and behavior graphs to provide further information about dynamics in the 3D scene.

A very interesting beginning in detecting salient frames for human skeleton datasets has been made by Assa *et al.* [2]. They generate an action synopsis for presenting the motion of a single skeleton-based character. They represent motion in affinity matrices, constructed from various aspects of a pose such as joint positions, joint velocities, joint angles, and joint angular velocities. They first define a vector $\mathbf{x_a^k}$ which represents an aspect a of the pose at frame k. Then, they compute the dissimilarity of the aspect a between two given frames i and j by a simple distance measure to identify key poses. Finally, they compose these key poses into a single image by including the most significant poses.

There has been a significant increase in research activities related to the visualization of molecular dynamics simulations. Lampe *et al.* explore the use of a two-level hierarchical technique for the visualization of protein dynamics [14]. Recently, Krone *et al.* presented a method capable of visualizing molecular surface dynamics at interactive rates [15]. Bidmon *et al.* present an informative and intuitive method for visualizing the motion of molecules around existing proteins using pathlines [16]. All of these papers [14–16] discuss methods for efficiently visualizing molecular dynamics, but do not detect key or salient frames int he simulation. Mehta *et al.* have explored approaches to the detection, classification and visualization of anomalous structures, such as defects in crystalline lattice structures [17, 18]. We are not aware of any research into the detection of salient frames for protein dynamics simulations.

3 Salient Frame Detection

In this paper, we define saliency as the uniqueness of a single frame with respect to its surrounding frames in time, and detect the salient frames for molecular dynamics simulations. Mechanosensitive ion channels play a critical role in transducing physical stresses at the cell membrane into an electrochemical response. The crystal structure of *E. coli* MscS has provided a starting point for detailed descriptions of its mechanism. Figure 3 shows the opening of the *E. coli* mechanosensitive ion channel that we will consider throughout this paper. There are 7 subunits in this ion channel, and all 7 subunits are topologically identical, but act relatively independently in the simulation. Each subunit has residues 1 to 175 (with few gaps cut out). To understand this mechanism, identifying the presence of kinks in α-helices is critical because they have functional importance. Kink detection, however, is a tricky question because there are many factors involved. These include the state (ruptured or not) of the H bonds, local geometric information such as Ramachandran angles (torsion angles), and more global information such as the angles among multiple atoms.

In this section, we formulate the relationship between one residue and the neighboring residues spatially, and present an algorithm to detect saliency in time. Our frame-

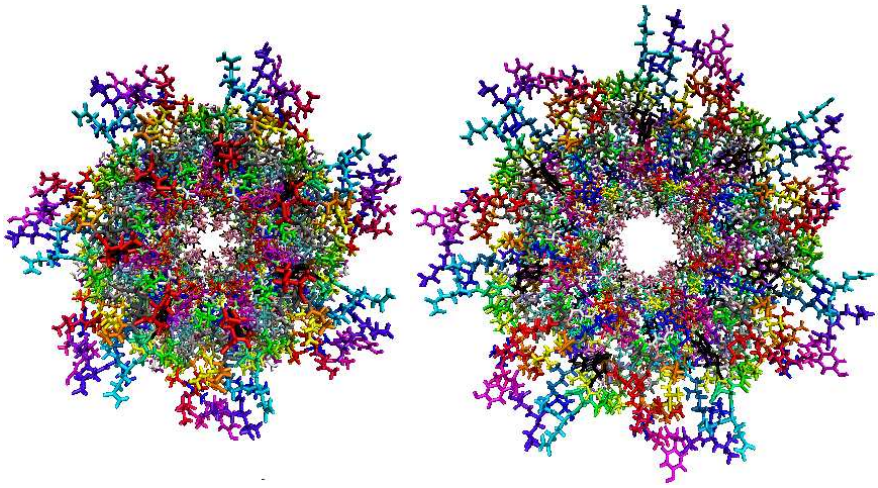

(a) (b)

Fig. 3: *The images above show the closed (left) and open (right) conformations of the heptameric* E. coli *mechanosensitive channel MscS.*

work encompasses the global and local geometric properties of backbone residues in a molecular dynamics simulation.

3.1 Construction of Affinity Matrices in Space

We explore the relationship between one residue and the neighboring residues to detect the changes in α-helices. The straightening and buckling of α-helices are interesting because they appear in many of simulations of ion channels and are believed to be correlated with conformational states of the whole channel. There are many ways to define the relationship among residues, but we believe the angles in backbone atoms would be one of the best ways since backbone atoms are much more stable in their positions than side-chains. As a Ramachandran plot suggests, we could have measured torsion (dihedral) angles and conjectured the changes of secondary structures for each residue. However, analysis of Ramachandran angles only considers very local properties inside a residue, and does not encompass the global geometric property among a sequence of residues. Instead, we use the relative angles between one C_α (α-carbon) and other α-carbons within a cut-off distance r_s.

Molecular dynamics simulation gives us a trajectory file which holds all the atom positions in 3D space for every frame k. Since three non-co-linear points in 3D space can define a plane, the positions of N-C_α-C atoms in each residue can define a plane and its normal vector n as shown in Figure 2(c). We first compute normal vectors (n_i) to the planes formed by these N-C_α-C atoms in residues (R_i) for every frame k. Then,

we construct an affinity matrix A_k for the k-th frame as:

$$A_k = \begin{bmatrix} n_1 \cdot n_1 & n_1 \cdot n_2 & n_1 \cdot n_3 & \dots & n_1 \cdot n_m \\ n_2 \cdot n_1 & n_2 \cdot n_2 & n_2 \cdot n_3 & \dots & n_2 \cdot n_m \\ n_3 \cdot n_1 & n_3 \cdot n_2 & n_3 \cdot n_3 & \dots & n_3 \cdot n_m \\ \vdots & \vdots & \vdots & \ddots & \vdots \\ n_m \cdot n_1 & n_m \cdot n_2 & n_m \cdot n_3 & \dots & n_m \cdot n_m \end{bmatrix} \quad (1)$$

where m is the number of residues that we consider. Here each element $a_k(i, j)$ is simply a dot product between the normals n_i and n_j. If two residues have indices i and j that differ by more than a cut-off value r_s, we set $a_k(i, j)$ to be zero. Throughout this paper, we use $r_s = 5$. Because on average, α-helices turn once every 3.6 amino acids, considering ± 5 amino acids forwards and backwards should cover, in total, about 3 turns in α-helices, which is a sufficient scale for kink detection.

Figure 4 visualizes the affinity matrices from the first and the second frames for 33 residues (from residue 94 to residue 126) of the subunit 1 for the molecule shown in Figure 3.

3.2 Saliency Detection among Neighboring Affinity Matrices

Our affinity matrix in equation 1 represents the geometric relationship among neighboring residues. This angular relationship cannot be represented by a single vector $\mathbf{x}$ as in [2]. Therefore, the dissimilarity between two given frames i and j should be computed by the difference between two affinity matrices A_i and A_j. There are several ways

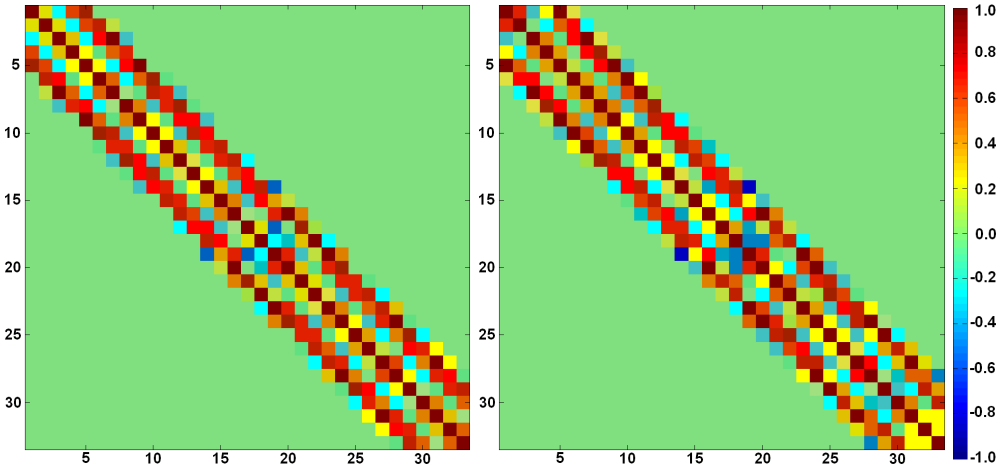

Fig. 4: *Visualization of affinity matrices computed from the first and the second frames for* 33 *residues of the subunit* 1 *for* E. coli *MscS (shown in Figure 3) when the cut-off distance,* $r_s = 5$ *is used.*

to compute the difference between two matrices. However, we have decided to use the singular value decomposition (SVD) in computing the difference between two matrices. The SVD [19] factorizes a given $m \times n$ matrix A into three matrices: $A = U \times \Sigma \times V^T$, where U is an $m \times m$ orthogonal matrix ($U \times U^T = I$ and $U^T \times U = I$), Σ is $m \times n$ diagonal matrix with non-negative numbers, and V^T is the transpose of an $n \times n$ orthogonal matrix V. There are two nice properties in the SVD decomposition: (1) The columns of U and V are a set of orthonormal basis vectors (singular vectors), and (2) the diagonal entries in Σ are called singular values, which are sorted in non-increasing order and indicate the importance of the corresponding basis vectors. If there is noise in the original matrix A, the least important basis vectors and singular values are dominated by noise and can be neglected.

In α-helices, backbone atoms (C, O, N, and H) are much more stable than side-chains because of the H bonds. However, there could be still a lot of vibrations in the positions of backbone atoms over time. By using SVD analysis, we can reduce the effects of vibrations by ignoring the smallest singular values. This is why we use SVD over other methods for computing the uniqueness of the affinity matrix A_i relative to the affinity matrix A_j.

Uniqueness of the affinity matrix A_i relative to the affinity matrix A_j: We perform a singular value decomposition on A_i: $A_i = U_i \times \Sigma_i \times V_i^T$. This returns the best basis vectors as the column vectors in U_i. Since the basis vectors are sorted by their importance in SVD decomposition, we can obtain a reduced matrix $\hat{U}_i$ by taking the first r_i basis vectors in U_i. For the j-th frame A_j, we use these r_i basis vectors to best approximate it. For this, we project A_j to the low-dimensional subspace spanned by the r_i basis vectors as: $W_{i,j} = \hat{U}_i^T \times A_j$. This gives us the weight matrix $W_{i,j}$ for the r_i basis vectors. We use this weight matrix to approximate A_j by: $\hat{A}_j = \hat{U}_i \times W_{i,j}$. Finally we compute the root mean square error (ε_{ij}) between $\hat{A}_j$ and A_j: $\| \hat{A}_j - A_j \|_F$, where the Frobenius norm of a matrix M is defined as $\| M \|_F = \sqrt{\sum_{i=1}^{m} \sum_{j=1}^{n} |l_{ij}|^2}$.

Saliency Value s_i for the frame i: To compute the uniqueness of a frame i relative to other frames j, we avoid considering all possible pairs (i, j). Instead, we consider neighboring frames j where $|i - j| \leq r_t$. Throughout this paper, we use $r_t = F/10$, where F is the total number of frames. The final saliency value s_i is the average of the errors ε_{ij} in neighboring frames of i:

$$s_i = \frac{\sum_{|j-i| \leq r_t} \varepsilon_{ij}}{F_i}$$

where F_i is the number of frames whose distance from the frame i is less than or equal to r_t. Figure 5 shows the graph for these saliency values in blue.

4 Results

We have compared our detected salient frames with the ones identified independently by our collaborators (biology scientists) for molecular dynamics simulations. Figure 5

shows the five most salient frames detected by our method for the subunit 4 in the *E. coli* mechanosensitive ion channel in Figure 3. The frames 5, 26, 30, and 34 which have been detected by our method are the same or very close to the frames 3, 24, 26, 30, and 35 with changes in the kinks, which were detected manually by our collaborators. The frame 39 detected by our algorithm is not close to any frame detected manually by our collaborators, but it had the lowest saliency value among the five most salient frames. Generally, kinks change towards the end of this simulation, and our method successfully detects these important frames.

Figure 6 shows the five most salient frames detected by our method for the subunit 1 in the ion channel shown in Figure 3. This subunit is topologically identical to the subunit 4, but acts differently in the simulation. Therefore, it results in different salient frames (frames 11, 19, 21, 35, and 39) as shown in Figure 6. Our collaborators identified frames 2, 18, 20, 23, 35, 36, and 39 as being salient. Figure 7 shows the six most salient frames detected by our method for the subunit 4 in the symmetry annealing of MscS F68S mutant. In this molecular dynamics simulation, residue 68 was mutated to another, serine, which has very specific consequences for channel inactivation in real experiments. As changes in the kinks occur more frequently than the previous simulations, we observe a larger number of salient frames than in the previous cases. Our collaborators have manually identified frames 2, 4, 18, 34, and 38 as being salient. Among these, frames 2, 4, 18, and 38 are the same or close to the frames 1, 5, 18, and 39 detected by our algorithm, and the remaining frame 34 also exhibits a relatively high saliency value as shown in Figure 7.

5 Conclusions and Future Work

In this paper, we have detected salient frames for molecular dynamics simulations. We have introduced the notion of saliency in time, and successfully identified most of the key frames which have changes in the kinks (i.e. appearance or disappearance of a kink) for *E. coli* channel. We believe that our method can enable researchers to focus on the important frames for further analysis of the dataset.

We currently consider the angles among residues in α-helices, and identify the anomalies (kinks) in the secondary structures for an *E. coli* channel. We believe, however, this framework can be easily extended to encompass salient features in other time-varying simulations by changing the way we construct affinity matrices to address other needs by scientists or domain experts. In this context, it will be interesting to compare and contrast the results of salient frames detected by a new method with what scientists think salient in their domains.

References

1. Johnson, C., Moorhead, R., Munzner, T., Pfister, H., Rheingans, P., Yoo, T.S.: NIH-NSF visualization research challenges report. Technical report, Mitsubishi Electric Research Laboratories (2006) Computing in Science and Engineering,.
2. Assa, J., Caspi, Y., Cohen-Or, D.: Action synopsis: pose selection and illustration. ACM Transactions on Graphics (Proceedings of ACM SIGGRAPH) **24**(3) (2005) 667–676

3. Joshi, A., Rheingans, P.: Illustration-inspired techniques for visualizing time-varying data. In: IEEE Visualization. (2005) 679–686
4. Turk, G., Banks, D.: Image-guided streamline placement. In: Proceedings of SIGGRAPH 1996. (1996) 453–459
5. Itti, L., Koch, C., Niebur, E.: A model of saliency-based visual attention for rapid scene analysis. IEEE Trans. on Pattern Analysis and Machine intelligence **20**(11) (1998) 1254–1259
6. Lee, C.H., Varshney, A., Jacobs, D.: Mesh saliency. ACM Trans. on Graphics (Procs. ACM SIGGRAPH) **24, No. 3** (2005) 659 – 666
7. Akitake, B., Anishkin, A., Liu, N., Sukharev, S.: Straightening and sequential buckling of the pore-lining helices define the gating cycle of mscs. Nature Structural and Molecular Biology **14**(12) (2007) 1141–1149
8. Branden, C., Tooze, J.: Introduction to Protein Structure. Second edn. Garland Publishing, Inc. (1999)
9. Ramachandran, G.N., Ramakrishnan, C., Sasisekharan, V.: Stereochemistry of polypeptide chain configurations. Journal of Mol. Biol. **7** (1963) 95–99
10. Anishkin, A., Sukharev, S.: State-stabilizing interactions in bacterial mechanosensitive channel gating and adaptation. The Journal of Biological Chemistry **284**(29) (Jul 2009) 19153–19157
11. McCloud, S.: Understanding Comics – The Invisible Art. Harper Perennial (1994)
12. Nienhaus, M., Dollner, J.: Depicting dynamics using principles of visual art and narrations. IEEE Computer Graphics and Applications **25**(3) (2005) 40–51
13. Pingali, G., Opalach, A., Jean, Y., Carlbom, I.: Visualization of sports using motion trajectories: Providing insights into performance, style, and strategy. In: Proceedings Visualization 2001. (2001) 75–82
14. Lampe, O.D., Viola, I., Reuter, N., Hauser, H.: Two-level approach to efficient visualization of protein dynamics. IEEE Transactions on Visualization and Computer Graphics **13**(6) (2007) 1616–1623
15. Krone, M., Bidmon, K., Ertl, T.: Interactive visualization of molecular surface dynamics. IEEE Transactions on Visualization and Computer Graphics **15**(6) (2009)
16. Bidmon, K., Grottel, S., Bs, F., Pleiss, J., Ertl, T.: Visual abstractions of solvent pathlines near protein cavities. **27**(3) (2008) 935–942
17. Mehta, S., Hazzard, K., Machiraju, R., Parthasarathy, S., Wilkins, J.: Detection and visualization of anomalous structures in molecular dynamics simulation data. In: VIS '04: Proceedings of the conference on Visualization '04, Washington, DC, USA, IEEE Computer Society (2004) 465–472
18. Mehta, S., Barr, S., Choy, A., Yang, H., Parthasarathy, S., Machiraju, R., Wilkins, J.: Dynamic classification of defect structures in molecular dynamics simulation data. In: Proceedings of SIAM on Data Mining. (2005)
19. Golub, G.H., Van Loan, C.F.: Matrix computations (3rd ed.). Johns Hopkins University Press, Baltimore, MD, USA (1996)

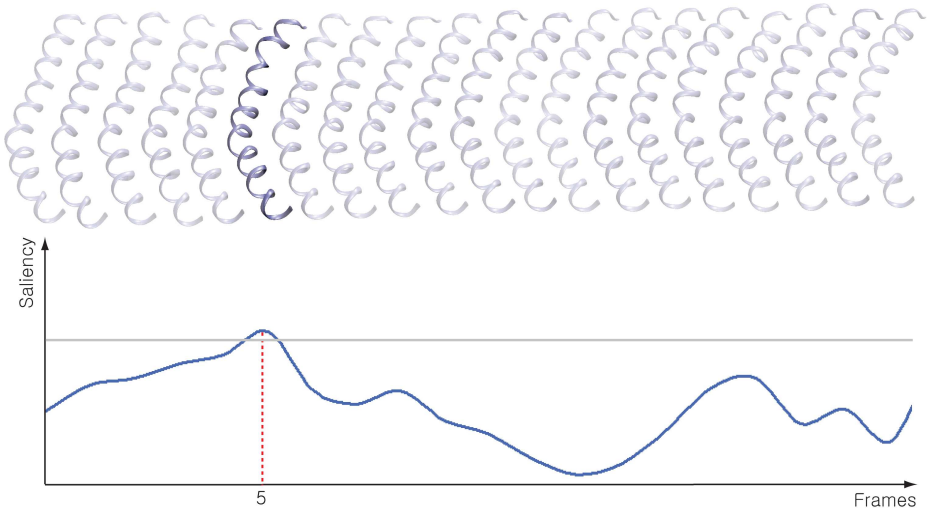

(a) Frames 0 to 19

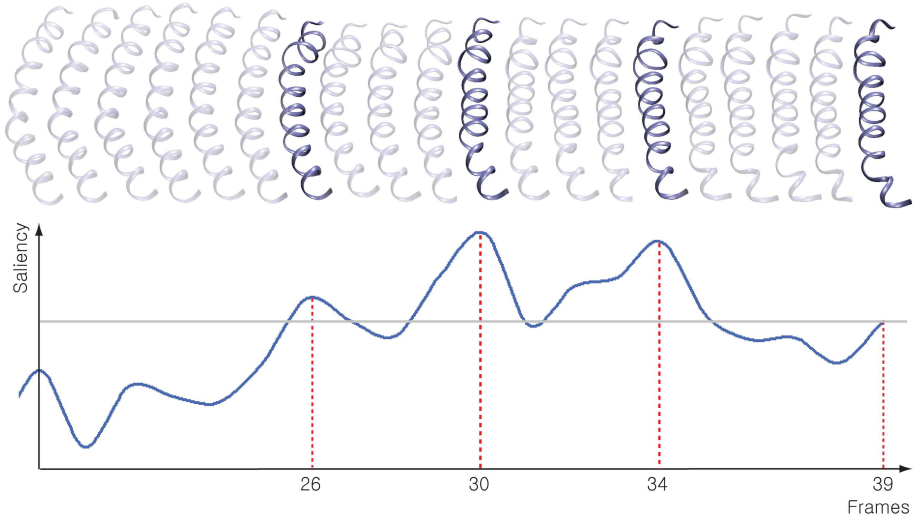

(b) Frames 20 to 39

Fig. 5: *Five most salient frames detected by our method for the subunit* 4 *in the* E. coli *ion channel (MscS) in Figure 3. The changes in the kinks are detected towards the end of this simulation, and our method successfully detects some of the most important frames.*

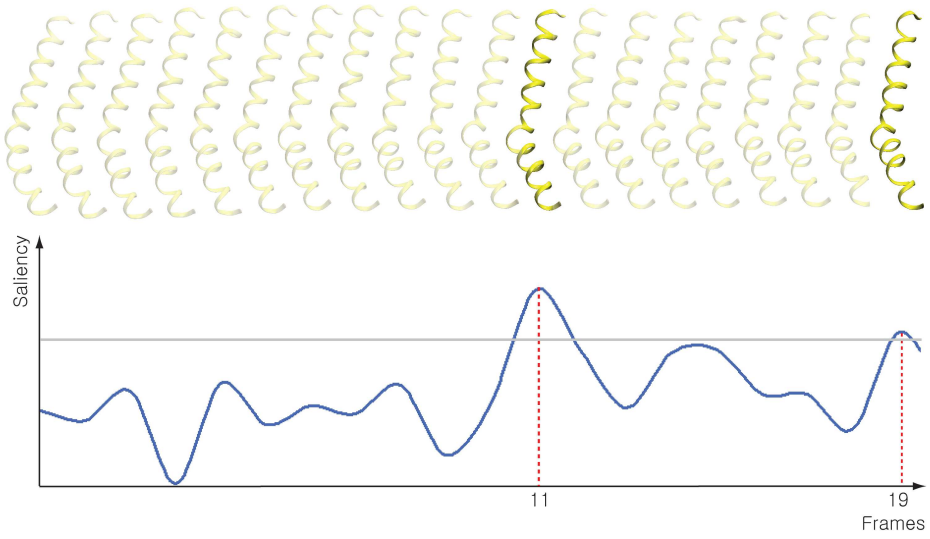

(a) Frames 0 to 19

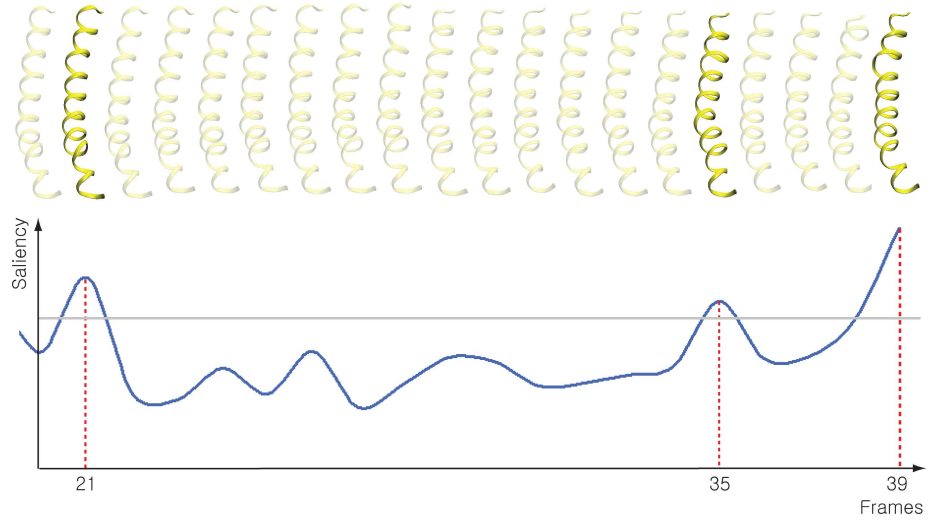

(b) Frames 20 to 39

Fig. 6: *Five most salient frames detected by our method for the subunit* 1 *in the* E. coli *ion channel (MscS) in Figure 3. This subunit is topologically identical to the subunit* 1*, but acts differently in the simulation.*

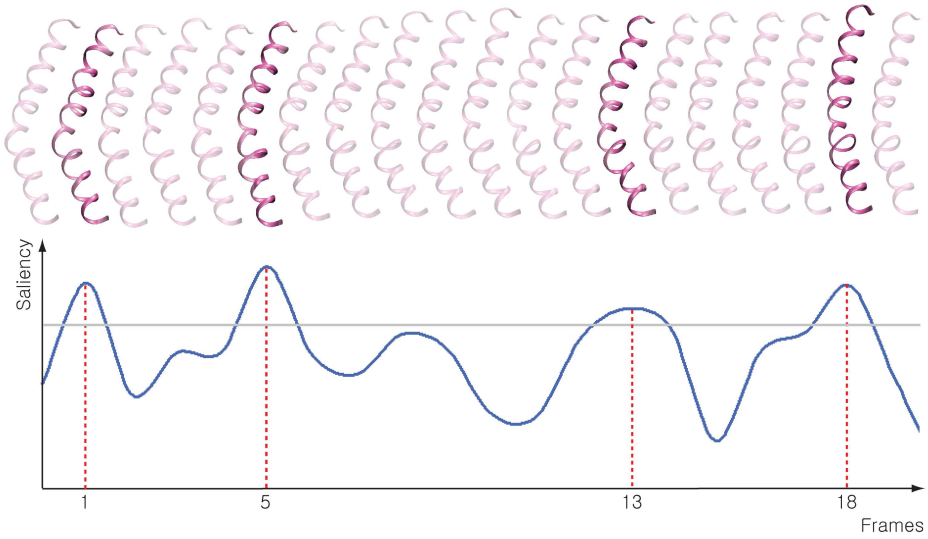

(a) Frames 0 to 19

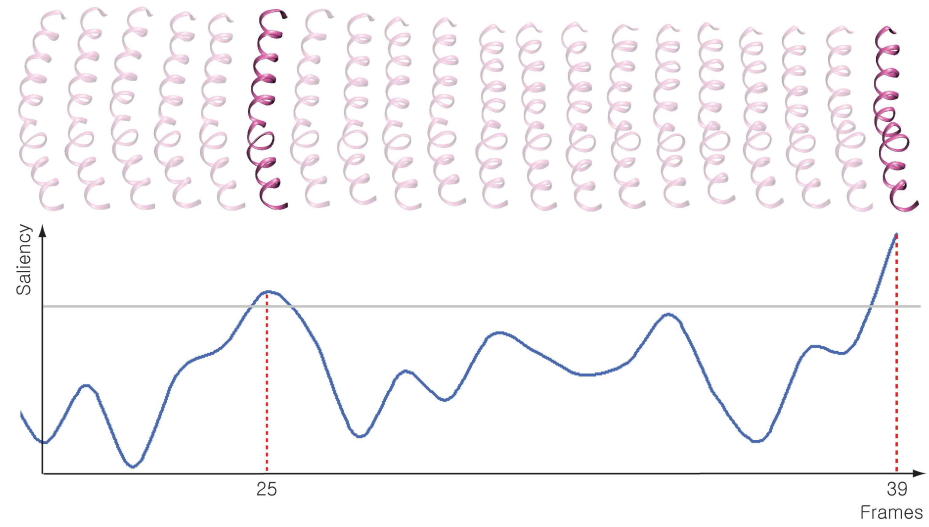

(b) Frames 20 to 39

Fig. 7: *Six most salient frames detected by our method for the subunit* 4 *in the other molecular dynamics simulation, showing the symmetry annealing of MscS F68S mutant – the residue* 68 *was mutated to another, serine, which has very specific consequences for channel inactivation in real experiments.*